JOURNAL OF COMPUTATIONAL PHYSICS 88, 255–283 (1990)

A Method for Solving Three-Dimensional Viscous Incompressible Flows over Slender Bodies

MOSHE ROSENFELD,* MOSHE ISRAELI, AND MICHA WOLFSHTEIN

Technion–Israel Institute of Technology, Haifa, Israel

Received February 5, 1988; revised March 31, 1989

A marching iterative method for solving the three-dimensional incompressible and steady reduced Navier–Stokes equations in general orthogonal coordinate systems is described with the velocity and the pressure as dependent variables. The coupled set of the linearized finite-difference continuity and momentum equations are solved iteratively without any splitting or factorization errors. Each iteration consists of spatial marching from the upstream boundary to the downstream boundary. The discrete continuity and the two linearized crossflow momentum equations are satisfied at each marching step, even when the mainstream momentum equation is not converged. This solution procedure is equivalent to the solution of a single Poisson-like equation by the successive plane over relaxation method, while other available solution methods employ a Jacobi-type iterative scheme and therefore are less efficient. Several properties of the numerical method have been assessed through a series of tests performed on the laminar incompressible flow over prolate spheroids at intermediate incidence.

1. INTRODUCTION

The ability to efficiently compute complicated three-dimensional, viscous, incompressible flows over slender bodies is of great importance to contemporary aerodynamics. Several methods are available for solving the compressible Navier–Stokes equations. The algorithm for the numerical solution of the three-dimensional incompressible Navier–Stokes equations are less well developed. One reason for this situation is the absence of a pressure time derivative in the continuity equation. Some approaches to overcome this issue have been suggested. In the artificial compressibility method [2, 8] a fictitious pressure time derivative, which vanishes at the steady state, is added to the continuity equation. In the fractional-step method [3, 5, 7] each time step is split into two or more stages. Usually, in the first stage the momentum equations are solved for an approximate value of the velocity. In the second step, the pressure field, which corresponds to a divergence-free velocity, is computed and the velocity field is accordingly corrected.

The computational cost of the solution of the three-dimensional Navier–Stokes equations is rather high. Therefore, simpler and more economical models of viscous

* Presently, Tel Aviv University, Ramat Aviv, Israel.

0021-9991/90 $3.00

flows have been sought. The well-known boundary layer equations are an asymptotic approximation of the Navier–Stokes equations for high Reynolds number flows. This approximation imposes the pressure field from an outer solution and neglects all diffusion terms except in the normal direction. The boundary layer equations are parabolic and therefore can be solved efficiently by marching methods, see for example Ref. [16]. Good results have been obtained in most three-dimensional boundary layer computations for attached flow regions. However, mathematical and numerical instabilities have been detected near the anticipated location of separation lines and no solutions could be obtained in flow-separated regions.

The singular behavior of the boundary layer solutions may be resolved by applying inverse methods. Van Dalsem and Steger [18] have solved the unsteady boundary layer equations for the flow over a 6:1 spheroid at an incidence of 30° by specifying the wall shear instead of the outer pressure in flow separated zones. No singular behavior was found near the separation line.

Interactive boundary layer schemes are popular for solving two-dimensional weakly separated flow regions, e.g., Veldman [19]. In these methods, the solution of the outer flow is coupled with the viscous flow solution. In order to circumvent the singularity of the boundary layer equation near separation, the inverse formulation should be used to solve the separated region. The extension of the method to three-dimensional flows is difficult, see Bodonyi and Duck [1] and it is not obvious whether the three-dimensional interactive boundary layer solution is more efficient than the solution of the whole flowfield by a more complete mathematical model. Moreover, the validity of the boundary layer approximation in regions with extensive flow separation is questionable.

The reduced Navier–Stokes (RNS) and the thin layer (TL) approximations occupy the middle ground between the Navier–Stokes equations and the boundary layer equations. In the RNS approximation the diffusion terms are neglected along one coordinate line which approximately coincides with the mainstream direction. In the TL approximation the circumferential diffusion is neglected as well, and only the diffusion terms normal to the body are retained. However, unlike the boundary layer approximation, the pressure field is not predetermined but is one of the unknowns in both the TL and the RNS approximations. Rubin [12] showed for high Reynolds number flows that the RNS equations contain all the important terms of the Navier–Stokes equations. Rosenfeld [9] showed for the incompressible case that the RNS and TL equations are still elliptic, although of reduced order. Therefore, both the RNS and the TL equations do not suffer from any mathematical or numerical singularities and for slender bodies they yield solutions which are very similar to those obtained from the Navier–Stokes equations.

In the artificial compressibility or fractional-step methods, the reduced ellipticity of the steady incompressible TL or RNS equations cannot be fully exploited to save computational resources, since these methods essentially advance the solution in time (either real or fictitious). Minor savings are obtained only due to fewer algebraic operations required for the computation of the viscous terms. Rubin and

Lin [13] have proposed for the two-dimensional case a solution method which takes advantage of the simplified character of the equations. The elliptic RNS differential equations are discretized by forward differencing of the streamwise pressure gradient and backward differencing of the streamwise convection terms. This discretization is consistent with the mathematical character of the RNS equations.

Unlike other incompressible methods of the primitive equations, the discrete coupled continuity *and* momentum equations are solved without any modification or reformulation of the continuity equation. "Global iterations" are used to solve iteratively the set of the algebraic equations. Each global iteration consists of marching line by line from the upstream boundary to the downstream boundary. On each marching step, the coupled set of the discrete continuity and momentum equations along the lines normal to the marching direction are solved simultaneously.

Israeli and Lin [4] improved for the two-dimensional case the convergence properties of the method by modifying the discrete streamwise momentum equation during the iterative solution procedure. The efficiency of the modified method stems from its equivalence to the iterative solution of a single two-dimensional elliptic equation by the successive line over relaxation (SLOR) procedure, while the fractional step or artificial compressibility methods, as well as the original method of Rubin and Lin [13] are equivalent to a Jacobi-type method. For a two-dimensional case, Rubin and Reddy [14] and Rosenfeld and Israeli [10] exploited the improved smoothing properties of the modified method to accelerate the convergence of the global iterations by a multigrid procedure.

The extension of that method, which directly couples the solution of the continuity and the momentum equations, to the three-dimensional case is non-unique. The present work suggests such an extension for solving the three-dimensional, viscous, incompressible, and steady reduced Navier–Stokes equations in generalized orthogonal coordinate systems. The method takes advantage of the reduced ellipticity of the equations to enhance the efficiency of the solution procedure by devising a three-dimensional iterative scheme which is equivalent to the solution of a single Poisson equation by the successive plane over relaxation method. The properties of the method are discussed in the light of some numerical experiments. It has been found that this method may be a good alternative for the solution of the steady incompressible reduced Navier-Stokes equations. It offers better efficiency than the fractional-step or the artificial compressibility methods due to improved convergence rate and lower storage requirements.

2. Mathematical Formulation

The RNS equations are written in a general axisymmetric curvilinear and orthogonal coordinate system using primitive variables. The three orthogonal coordinates ρ, θ, and ξ run approximately in the normal, circumferential, and

mainstream directions respectively, see Fig. 1. One-dimensional stretching functions are used to define a modified coordinate system q, s, t, where grid points can be clustered in high gradient flow reegions without losing orthogonality. The restriction of axisymmetric coordinates is made to simplify the coding and reduce computer resources. The method itself is applicable to general orthogonal coordinate systems without any modifications.

The physical components of the velocity in the coordinate directions, (V_q, V_s, V_t), are scaled according to

$$u = h_q V_q, \qquad v = h_s V_s, \qquad w = h_t V_t, \tag{1}$$

where h_q, h_s, h_t are the Lámme coefficients. The scaled velocity components (u, v, w) are equal to the contravariant components of the velocity, multiplied by the square of the corresponding Lámme coefficients, e.g., $u = h_q^2 U^q$, where U^q is the contravariant velocity component along q.

In an orthogonal coordinate system, the mixed derivatives in the diffusion terms can be eliminated by using the continuity equation. The resulting non-dimensional laminar RNS equations for an incompressible and isothermal flow consist of the continuity equation

$$\frac{\partial(\sigma u)}{\partial q} + \frac{\partial(\tau v)}{\partial s} + \frac{\partial(\delta w)}{\partial t} = 0, \tag{2}$$

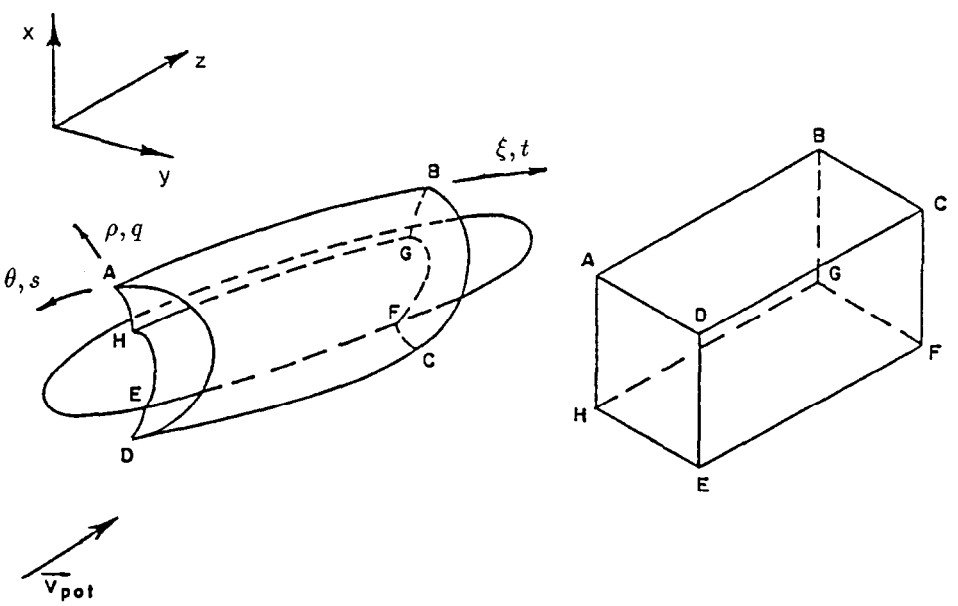

FIG. 1. The coordinate system and the computational domain.

and the momentum equations in the q, s, t directions, respectively,

$$\begin{aligned}
&\frac{1}{h_q}\left(\sigma u\frac{\partial}{\partial q}\left(\frac{u}{h_q}\right)+\tau v\frac{\partial}{\partial s}\left(\frac{u}{h_q}\right)+\delta w\frac{\partial}{\partial t}\left(\frac{u}{h_q}\right)\right)+\frac{1}{2}\left(\delta\frac{\partial\beta}{\partial q}v^2+\sigma\frac{\partial\gamma}{\partial q}w^2-\delta\frac{\partial\alpha}{\partial t}uv\right)\\
&\quad=-\sigma\frac{\partial P}{\partial q}+\frac{1}{\mathrm{Re}}\left(\frac{\partial}{\partial q}\left(\alpha\frac{\partial}{\partial q}(\sigma u)\right)+\frac{1}{\delta}\frac{\partial^2 u}{\partial s^2}+\frac{\partial}{\partial q}\left(\frac{1}{\delta}\right)\frac{\partial v}{\partial s}-\frac{\partial}{\partial q}\left(\delta\frac{\partial\alpha}{\partial t}w\right)\right),\\
&\frac{1}{h_s}\left(\sigma u\frac{\partial}{\partial q}\left(\frac{v}{h_s}\right)+\tau v\frac{\partial}{\partial s}\left(\frac{v}{h_s}\right)+\delta w\frac{\partial}{\partial t}\left(\frac{v}{h_s}\right)\right)-\frac{1}{2}\left(\delta\frac{\partial\beta}{\partial t}vw+\sigma\frac{\partial\beta}{\partial q}uv\right)\\
&\quad=-\tau\frac{\partial P}{\partial s}+\frac{1}{\mathrm{Re}}\left(\frac{\partial}{\partial q}\left(\frac{1}{\delta}\frac{\partial v}{\partial q}\right)+\tau\beta\frac{\partial^2 v}{\partial s^2}-\delta\frac{\partial\beta}{\partial t}\frac{\partial w}{\partial s}-\sigma\frac{\partial\beta}{\partial q}\frac{\partial u}{\partial s}\right),\qquad(3)\\
&\frac{1}{h_t}\left(\sigma u\frac{\partial}{\partial q}\left(\frac{w}{h_t}\right)+\tau v\frac{\partial}{\partial s}\left(\frac{w}{h_t}\right)+\delta w\frac{\partial}{\partial t}\left(\frac{w}{h_t}\right)\right)+\frac{1}{2}\left(\delta\frac{\partial\beta}{\partial t}v^2+\delta\frac{\partial\alpha}{\partial t}u^2-\sigma\frac{\partial\gamma}{\partial q}uv\right)\\
&\quad=-\delta\frac{\partial P}{\partial t}+\frac{1}{\mathrm{Re}}\left(\frac{\partial}{\partial q}\left(\frac{1}{\tau}\frac{\partial w}{\partial q}\right)+\frac{1}{\sigma}\frac{\partial^2 w}{\partial s^2}+\frac{\partial}{\partial q}\left(\frac{\partial}{\partial t}\left(\frac{1}{\tau}\right)u\right)+\frac{\partial}{\partial t}\left(\frac{1}{\sigma}\right)\frac{\partial v}{\partial s}\right),
\end{aligned}$$

where

$$\begin{aligned}
&\alpha=\frac{1}{h_q^2},\qquad \beta=\frac{1}{h_s^2},\qquad \gamma=\frac{1}{h_t^2},\\
&\sigma=\alpha J,\qquad \tau=\beta J,\qquad \delta=\gamma J,
\end{aligned}\qquad(4)$$

and the Jacobian J is given by

$$J=h_q h_s h_t.\qquad(5)$$

A characteristics analysis of the three-dimensional RNS equations [9] reveals that it has *two elliptic* and *four parabolic* characteristics. Therefore, the three-dimensional RNS equations are equivalent to a system of *one second-order elliptic* equation and *two second-order parabolic* equations and are well posed if three boundary conditions are specified on all boundaries, except at the downstream boundary where only one condition is required. In comparison, the Navier–Stokes equations have *six elliptic* characteristics and therefore require three boundary conditions on *all* boundaries. The proper number of boundary conditions should be chosen from the three velocity components and the pressure.

In the present work only external flows over a body are considered. Out of the possible set of boundary conditions, the following are chosen. At the upstream boundary (denoted by the subscript "up"), the three components of the velocity are specified (for example, from a boundary layer computation)

$$u=u_{\mathrm{up}},\qquad v=v_{\mathrm{up}},\qquad w=w_{\mathrm{up}}.\qquad(6a)$$

The downstream boundary is usually an outflow boundary where in many applica-

tions the conditions are not known. One of the advantages of the RNS approximation is that only one condition should be specified there. The streamwise derivative of the pressure is a simple choice,

$$\frac{\partial P}{\partial t} = \left(\frac{\partial P}{\partial t}\right)_{\text{pot}}, \tag{6b}$$

where the subscript "pot" stands for the potential value.

Three boundary conditions should be specified at the outer boundary. The admissible conditions depend strongly on the location of the boundary. If the outer boundary is very far from the solid body, a uniform velocity may be specified there. For high Reynolds number flows, the distance between the outer boundary and the body can be decreased and some saving in the required number of mesh points may be achieved, if the velocity is specified from the inviscid solution, e.g., from a potential solution. If the boundary is placed inside the region of strong viscous–inviscid interaction, the prescription of the pressure may produce numerical instabilities similar to the singularity found in the boundary layer approximation near flow separated zones. However, this singularity results from the boundary conditions and is not an inherent property of the differential equations.

In the present study we assume that the outer boundary is in a potential flow region. We chose to specify the streamwise and circumferential velocity components and the pressure

$$v = v_{\text{pot}}, \qquad w = w_{\text{pot}}, \qquad P = P_{\text{pot}}. \tag{6c}$$

The normal scaled velocity component u is not given at this boundary. Thus, the displacement effect due to the development of the viscous boundary layer is computed rather than prescribed and it can be used as a driving mechanism for a viscous–inviscid interaction algorithm.

At a solid surface, the no-slip and the no-injection conditions are enforced

$$u = v = w = 0. \tag{6d}$$

Other boundaries may include periodic or symmetry boundaries.

3. Discretization

The differential equations are discretized by finite-differences. A uniform mesh is spread over the computational domain (q, s, t) with indices (i, j, n) and mesh size $(\Delta q, \Delta s, \Delta t)$, respectively. The variables are defined in a staggered location as shown in Fig. 2. The pressure is not defined at the center of the computational cell, as is usually done in fractional-step methods, but at the same point as the streamwise velocity component w. This arrangement has been used by Rosenfeld and Israeli [10] in a two-dimensional problem for obtaining second-order accuracy in the streamwise direction as well.

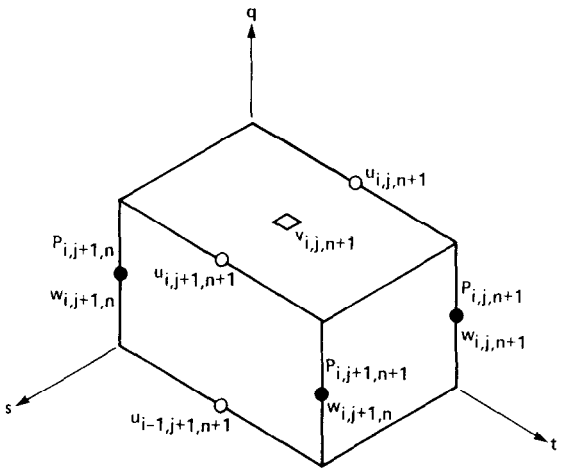

FIG. 2. The definition of the variables in the staggered grid.

The continuity equation is approximated at the center of each computational cell by a second-order central approximation

$$\frac{\sigma_{n+1/2}u-\sigma_{i-1,n+1/2}u_{i-1}}{\Delta q}+\frac{\tau_{n+1/2}(v-v_{j-1})}{\Delta s}+\frac{\delta w-\delta_n w_n}{\Delta t}=0. \tag{7}$$

For simplicity, the default indices i, j, and $n+1$ are omitted whenever no ambiguity arises. The momentum equations are discretized in a staggered grid and the resulting algebraic equations can be written as

$$A_{n+1/2}\frac{V-V_n}{\Delta t}=\theta_c\,\mathscr{L}V+(1-\theta_c)\,\mathscr{L}_n V_n+\mathscr{S}_{n+1/2}\,V_{n+1/2}+G_n P_n+\mathscr{C}_{n+1}, \tag{8}$$

where $V_n=(u_n, v_n, w_n)^{\mathrm{T}}$. The matrix $A_{n+1/2}$ includes terms which result from the streamwise convection, while $\mathscr{L}_n$ and $\mathscr{S}_{n+1/2}$ include the crossflow convection and diffusion terms, and the source terms, respectively. The vector $G_n P_n$ results from the pressure gradient term and $\mathscr{C}_{n+1}$ includes the boundary conditions as well as the pressure at the station $n+1$, but only in the t-momentum equation. In regions where the w-component velocity is reversed, $\mathscr{C}_{n+1}$ contains also the velocity components at the downstream station $n+1$.

The centering of the crossflow velocity derivatives along the t-direction in the momentum equations (8) is determined by the parameter θ_c. The values $\theta_c=0$ and $\theta_c=1$ correspond to calculating $\mathscr{L}V$ at the upstream station n (forward Euler scheme) or at the downstream station $n+1$ (backward Euler scheme), respectively. Only the choice $\theta_c=\frac{1}{2}$ (Crank–Nicholson scheme) results in a second-order accurate scheme in the t-direction. In the present application, the value $\theta_c=1$ has been chosen to enhance the stability properties of the scheme (see Section 5.2), at the expense of losing second-order accuracy in the t-direction.

A second-order central difference approximation of the pressure derivatives can be obtained from

$$\left(\sigma \frac{\partial P}{\partial q}, \tau \frac{\partial P}{\partial s}, \delta \frac{\partial P}{\partial t}\right) = \left(\frac{\sigma_n}{\Delta q}(P_{i+1,n} - P_n), \frac{\tau_n}{\Delta s}(P_{j+1,n} - P_n), \frac{\delta_{n+1/2}}{\Delta t}(P_{n+1} - P_n)\right), \tag{9}$$

due to the staggering of the momentum equations. This approximation, along with the approximation of the continuity equation (7), is consistent in the sense that the regular seven-point finite difference stencil of the underlying equivalent Poisson equation for the pressure may be derived discretely. Note, however, that in the present method a Poisson equation (which in some methods replaces the continuity equation) is neither formulated nor explicitly solved.

The crossflow derivatives of the diffusion terms are approximated by second-order accurate central differences, while the crossflow derivatives of the convection terms are computed from

$$a \frac{\partial V}{\partial x} = a \frac{V_{m+1} - V_{m-1}}{2\Delta x} - \varepsilon a \frac{V_{m+1} - 2V_m + V_{m-1}}{2\Delta x} + O(\varepsilon \Delta x), \tag{10}$$

where a refers to any one of the velocity components (see Eqs. (3)), x is a crossflow coordinate (q or s), and m is the index along that coordinate. The parameter ε governs the amount of numerical diffusion (often called the implicit second-order smoothing term) added to enhance the stability properties for high Reynolds number flows. The value $\varepsilon = 0$ corresponds to second-order central approximation, while $\varepsilon = 1$, which has been chosen in most of the present computations, corresponds to first-order upwind differences. Second-order accuracy in the crossflow directions can be restored by choosing $\varepsilon = O(\Delta x)$. It should be emphasized that all the streamwise derivatives of the velocity, as well as the continuity equation and the pressure derivatives, are approximated by second-order central difference approximation without any artificial diffusion.

The non-linear difference equations have been linearized by a single Newton–Raphson iteration. The discrete equations are re-formulated so that the increment of the solution $\Delta\phi$ is the unknown

$$\Delta\phi = \phi_{n+1} - \phi_n, \qquad \text{where} \quad \phi_{n+1} = (u_{n+1}, v_{n+1}, w_{n+1}, P_n)^{\mathrm{T}}. \tag{11}$$

The unknown velocity components belong to the step $n+1$ while the unknown pressure is computed at the previous step n. It is a direct consequence of the mixed elliptic-parabolic character of the RNS equations. The pressure at the step $n+1$ introduces the elliptic nature of the differential equations into the discrete approximation. The difference equations for each crossflow plane of constant index n can be written as

$$M_n \Delta\phi = b_{n+1}, \tag{12}$$

where the unknown is $\Delta\phi$. The asymmetric coefficient matrix M_n depends only on terms from the crossflow plane n and has a structure similar to that resulting from a five-point discretization of a two-dimensional Poisson equation in an orthogonal coordinate system. However, each entry is a sub-matrix of order 4×4, corresponding to the four unknowns of each computational cell (u, v, w, P). The vector b^{n+1} depends on the downstream station $n+1$, since it includes the boundary conditions at that station and the pressure from the t-momentum equation, as well as the velocity in regions of reversed flow along the t-direction.

4. Solution Method

4.1. *The Plane Iterative Method*

The finite difference form (12), which is an outcome of the mathematical character of the RNS equations, can be utilized to devise an efficient iterative scheme. One posssibility is to solve *simultaneously* the sub-block of equations corresponding to each step $n = 1, 2, ..., \mathcal{N}$ by computing b^{n+1} from the previous iteration

$$M_n^{k+1} \Delta\phi^{k+1} = b_{n+1}^k, \tag{13}$$

where k is the iteration level. One complete sweep from the upstream boundary $n = 1$ to the downstream boundary $n = \mathcal{N}$ is usually called a "global iteration." The global iterations are repeated until the convergence of (13) is achieved for all n.

This solution method is equivalent to an iterative solution of a second-order three-dimensional elliptic equation for the pressure. The velocity components can be viewed as auxiliary variables which appear in the governing equations and in the boundary conditions. This hierarchy of the dependent variables in the RNS equations is a result of the existence of two elliptic characteristics, which correspond to a Poisson-like equation for the pressure, and four parabolic characteristics, which govern the nature of the velocity field. A significant reduction in the storage can be achieved since only one three-dimensional variable (the pressure field) must be stored while the velocity field is re-generated during the plane by plane marching process. Alternative solution methods require the storage of *four* three-dimensional fields (the pressure and the three velocity components).

The simultaneous solution of the finite difference equations at each crossflow plane has favorable effects on the numerical properties of the solution procedure. The discrete linearized crossflow momentum equations are satisfied to the convergence error of the plane equations, even when the *global iterations* have not yet converged, since their right-hand-side terms do not depend on the step $n+1$ (provided that no reversed velocity exists in the marching direction). The discrete continuity equation is *always* satisfied and no smoothing terms have been added to it. The global iterations are required to satisfy the mainstream momentum equation (which has P_{n+1} as an unknown).

4.2. *Modification of the Iterative Solution Method*

A good iterative solver of the finite difference equations should take advantage of the special mathematical character of the differential equations. The RNS equations are equivalent to a single second-order Poisson-like equation and to two second-order parabolic equations. The elliptic nature of the system is dominant, as far as the numerical properties are considered. Therefore, a well-constructed solver of the RNS equations should solve efficiently the underlying Poisson equation.

The algorithm described in the last section, which is an extension to the three-dimensional case of the scheme given by Rubin and Lin [13] and Rubin and Reddy [14], does not yield good convergence rate of the global iterations because it corresponds to an inefficient iterative solver of an elliptic equation. For the two-dimensional Cartesian case, Israeli and Lin [4] devised a modification which makes the iterative solution procedure equivalent to the solution of a single second-order elliptic equation by the SLOR method, with all its favorable numerical characteristics. This method was applied to two-dimensional curvilinear orthogonal coordinate systems by Rosenfeld and Israeli [10].

The extension of the method to the three-dimensional case has not been done yet. Actually, this extension is non-unique. The iterative scheme for the solution of the coupled momentum and continuity equations may be chosen from a wide variety of methods such as the SLOR method, ADI-like schemes or plane relaxation schemes. However, it is not always easy to equivalence the solution procedure to an efficient iterative solver of a second-order Poisson-like equation. The present work suggests that a relatively simple modification of the t-momentum equation may be devised if (12) is solved by the plane iterative method as described in the previous section. The finite-difference approximation of the pressure derivative in the t-momentum equation should be modified to

$$\left(\delta \frac{\partial P}{\partial t}\right)^k \approx \frac{\delta_{n+1/2}}{\Delta t}\left(P_{n+1}^{k-1} - P_n^*\right) + \frac{S_n}{\Delta t}. \tag{14a}$$

The first term in the left-hand side of (14a) is the usual central difference approximation (9), and the modification term S_n is defined recursively by

$$\begin{aligned} &n = 1, && S_1^k = 0 \\ &n = 2, 3, \ldots, \mathcal{N}, && S_n^k = S_{n-1}^k + \delta_{n-1/2}\left(P_n^{k-1} - P_n^* + P_{n-1}^k - P_{n-1}^*\right). \end{aligned} \tag{14b}$$

The unknown P_n^* is a temporary value. The final value of the pressure at station n for the k level iteration is computed from

$$P_n^k = \omega P_n^* + (1-\omega)\, P_n^{k-1}, \tag{14c}$$

where ω is an over-relaxation parameter. It can be easily verified that when convergence is achieved, $S_n \equiv 0$ for all n and therefore the original discrete t-momentum equation is recovered. The modification (14) has been devised so that the iterative

solution of the incomporessible three-dimensional RNS equations is equivalent to the successive plane over relaxation (SPOR) method for the solution of a single three-dimensional second-order elliptic equation. Additional details are given by Rosenfeld [9].

The convergence properties of the two-dimensional method have been studied by Rubin and Reddy [14] and by Rosenfeld and Israeli [10]. In the three-dimensional case, if the solution method (12) with the modification (14) is adopted, the numerical properties of the method are similar to the SPOR method. In particular, for $\omega = 1$ the maximal eigenvalue of the iteration matrix is

$$\lambda_{\max} \sim 1 - \frac{1}{4}\left(\frac{\pi \Delta L}{Y_m}\right)^2 \qquad \text{for} \quad \frac{\pi \Delta L}{Y_m} \ll 1, \tag{15}$$

where ΔL is the physical step size in the marching direction and Y_m is a typical dimension of the crossflow plane (see Rosenfeld [9]). For large enough $\pi \Delta L / Y_m$ (typical to high Reynolds number flows without massive separation) the convergence is very rapid. However, when $\pi \Delta L / Y_m$ is small the convergence may degrade and in some cases the global iterations would not converge due to nonlinear effects. Yet, Rosenfeld and Israeli [10] have found for two-dimensional cases that the application of a multigrid procedure can considerably enhance the convergence properties even for small $\pi \Delta L / Y_m$.

The simultaneous solution of the difference equations at each marching step improves the convergence properties of the global iterations but may require excessive computing time. Therefore, an efficient algorithm should be applied to the simultaneous solution of (12) for each n. In the present work, a version of the generalized minimal residual (GMRES) method [15, 20, 21] is used with an ADI block-factorization preconditioning. The GMRES method is a conjugate-gradient type method which is directly applicable to the present asymmetric coefficient matrix M, but requires large additional storage. Details on the application of the GMRES method are given in Appendix A.

Summary of the solution method.

(a) Guess a pressure field.

(b) Perform one global iteration:

(1) Start marching from the upstream crossflow station $n = 1$.

(2) Solve Eqs. (13) simultaneously for the crossflow station n by the GMRES method.

(3) Proceed to the next crossflow station $n = n + 1$ and repeat step (b2). If $n > \mathcal{N}$ the present global iteration is completed, goto step (c).

(c) If the convergence criterion of the global iterations is met, end iterations; else repeat step (b)

5. Numerical Experiments

Following a series of two-dimensional validation cases, the laminar flow over a prolate spheroid at incidence has been computed as a three-dimensional test case. The interest of the present study is focused on the investigation of the numerical properties of the method rather than the physical aspects of the flowfield.

An analytical orthogonal body-fitted coordinate system (ρ, θ, ξ) can be generated in this case,

$$\begin{aligned} X &= a \sinh \rho(q) \sin \xi(t) \cos \theta(s), \\ Y &= a \sinh \rho(q) \sin \xi(t) \sin \theta(s), \\ Z &= a \cosh \rho(q) \cos \xi(t), \end{aligned} \tag{16}$$

where (X, Y, Z) is the Cartesian coordinate system, $a = \sqrt{\tau^2 - 1}/\tau$, and τ is the major to minor axes ratio. The functions $\rho(q)$, $\xi(t)$ are given hyperbolic stretching functions and $\theta = \pi s$. The sections $\theta = 0°$ and $\theta = 180°$ correspond to the windward and to the leeward symmetry planes, respectively.

The computational domain covers most of the spheroid. The upstream boundary is placed some distance downstream of the forward stagnation point. The boundary condition there for the streamwise direction velocity component is approximated by a Karman–Pohlhausen velocity profile with a displacement thickness given from the integral boundary layer solution of Stock [17] of a similar case. The two crossflow components are specified from the potential solution. The downstream boundary is located ahead of the rear stagnation point. Here, the pressure derivative along the streamwise direction is specified from the potential solution. At the outer boundary the pressure and the circumferential and the streamwise velocity components are specified from the potential solution.

The quantities to be presented in the following sections are the pressure, the two components of the normalized skin-friction coefficient and an integral displacement-like thickness of the boundary-layer. The normalized skin-friction coefficient on the spheroid, $\mathbf{C}_f = (C_{f,\xi}, C_{f,\theta})$, is defined by

$$\mathbf{C}_f = \frac{\tau_w}{(1/2)\,\rho_\infty V_\infty^2} \sqrt{\mathrm{Re}}, \tag{17}$$

where τ_w is the skin friction vector on the surface, ρ_∞ is the (constant) density, V_∞ is the far upstream uniform velocity, and Re is the Reynolds number (based on the major axis of the spheroid). Among several possibilities, the integral thickness δ^* is defined by

$$\delta^* = \sqrt{\mathrm{Re}} \int_0^1 \left(1 - \frac{V_t}{(V_t)_{\rho = \rho_{\mathrm{out}}}}\right) h_q \, dq, \tag{18}$$

where $(V_t)_{\rho = \rho_{\mathrm{out}}}$ is the value of the t-component velocity at the outer boundary.

The remainder of this chapter will elaborate on some numerical experiments which have been performed to investigate the properties of the scheme (13)–(14). Additional results and comparisons with other numerical and experimental works are given in Refs. [9, 11]. Section 5.1 presents numerical experiments for assessing the importance of the simultaneous solution of the difference equations at each marching step, as well as some properties of the global iterations. Section 5.2 elaborates on the spatial accuracy of the scheme and Section 5.3 discusses the effect of the boundaries location on the solution. Section 5.4 gives sample results for the flowfield over a prolate spheroid at incidence.

5.1. *Iterative Solution of the Discrete Equations*

difference equations (13) at each marching station is essential for ensuring accurate solution and favorable convergence properties of the global iterations. This was clearly demonstrated by attempts to solve (13) only approximately by an *iterative* block-ADI method (without using the GMRES method), rather than solving it simultaneously. Figure 3 shows the skin-friction coefficient and the integral thickness as a function of the number of ADI iterations KMAX performed at each marching step (an identical global convergence criterion has been used in all cases). The choice KMAX = 1 corresponds to marching along the mainstream direction by an ADI method. Greater values of KMAX result in more accurate solutions at each step because the splitting errors of the iterative ADI method decrease with increasing KMAX. As Fig. 3 demonstrates, the solution obtained by an ADI marching scheme (KMAX = 1) is quite different from the solutions obtained for KMAX = 4 and KMAX = 7, where the solution of (13) is more accurate. The differences in the results are significant, especially in the circumferential component of the skin friction. Further experiments prove that the inaccurate solution of (13) (large splitting errors) may introduce oscillations, especially near a solid wall and when strong circumferential reversed flow exists. Consequently, Eq. (13) is solved simultaneously in all the following computations by the GMRES method with a convergence criterion of 10^{-8} (based on the $L2$-norm of $\Delta\phi$).

The convergence history of the global iterations for the flow over two spheroids of axes ratio 6:1 and 4:1 at 10° incidence and Reynolds number of 10^6 is shown in Fig. 4. A grid of $24 \times 24 \times 32$ mesh points is used in the ρ, θ, and ξ directions, respectively. The ρ coordinate value at the spheroid surface and at the outer boundary is ROIN and ROUT, respectively. The global iteration convergence error ε is defined by

$$\varepsilon = N^{1/3} \sqrt{\sum (P^{(k)} - P^{(k-1)})^2}, \tag{19}$$

where N is the total number of mesh points. This definition is adapted from multigrid practices and is different from the usual $L2$-norm definition (here the sum of the squares is multiplied by $N^{1/3}$ rather than divided by N and therefore the present criterion is more stringent). In accordance with the prediction of (15), the con-

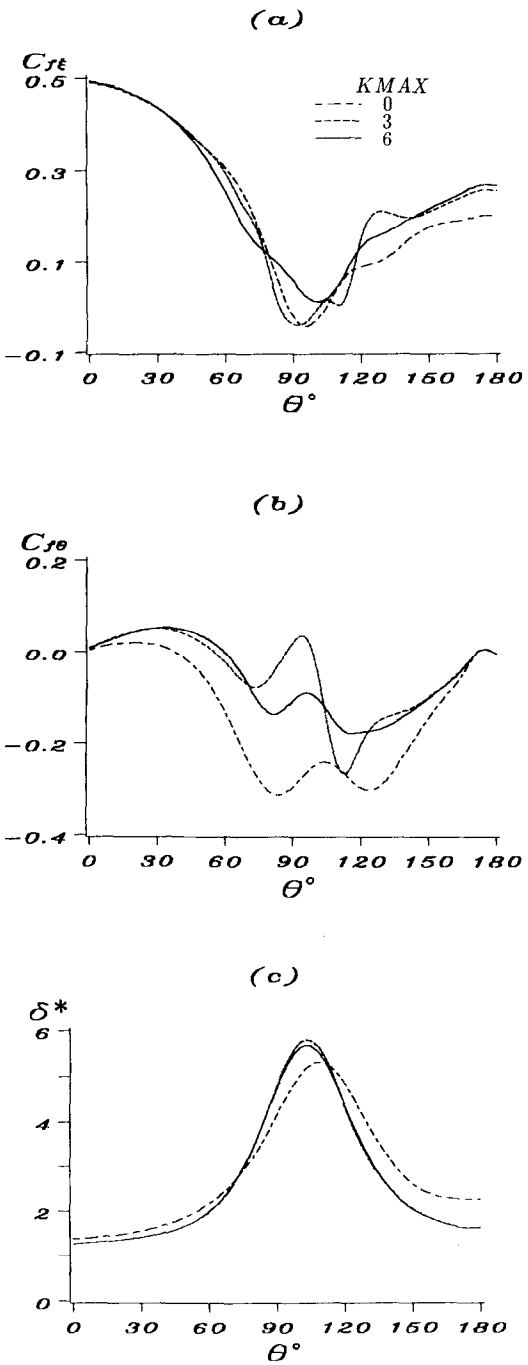

FIG. 3. The effect of the inaccurate solution of the plane equations (GMRES is not used).

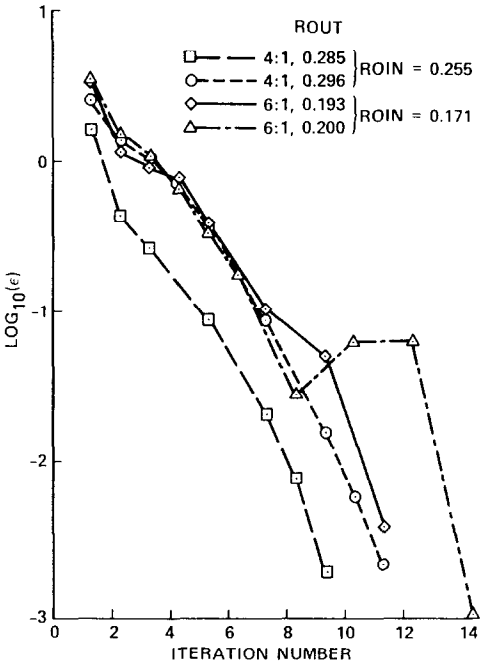

FIG. 4. Convergence history of the global iterations.

vergence rate worsens as the distance between the outer and the inner boundary increases. The convergence may not be monotonic and might even deteriorate if the outer boundary is far from the spheroid. This limitation is not severe for high Reynolds number flows without massive separation—e.g., when the flow is confined to a relatively thin region around the body. The computation for lower Reynolds numbers or for flows with large separated regions would require a multigrid procedure to obtain reasonable convergence rate, see Rosenfeld and Israeli [10]. Figure 5 reveals no need to choose very small values of the global iteration's convergence criterion ε. Usually 10–20 global iterations are required to achieve convergence ($\varepsilon < 10^{-8}$). The CPU time is 1 to 2 hr on the IBM 3081D scalar computer.

5.2. *Accuracy Tests*

The pressure derivatives and the streamwise velocity derivatives in the momentum equations, as well as the velocity derivatives in the continuity equation are approximated by central second-order-accurate differences. However, to enhance the stability properties of the marching scheme and to remove sensitivity to the upstream boundary conditions, the streamwise centering of the crossflow velocity derivatives are backward approximated by choosing $\theta = 1$ in (8). This degrades the accuracy of the scheme to first-order in the t-direction. Extensive convergence tests have been conducted for successively refined grids in the t-direction. Linear con-

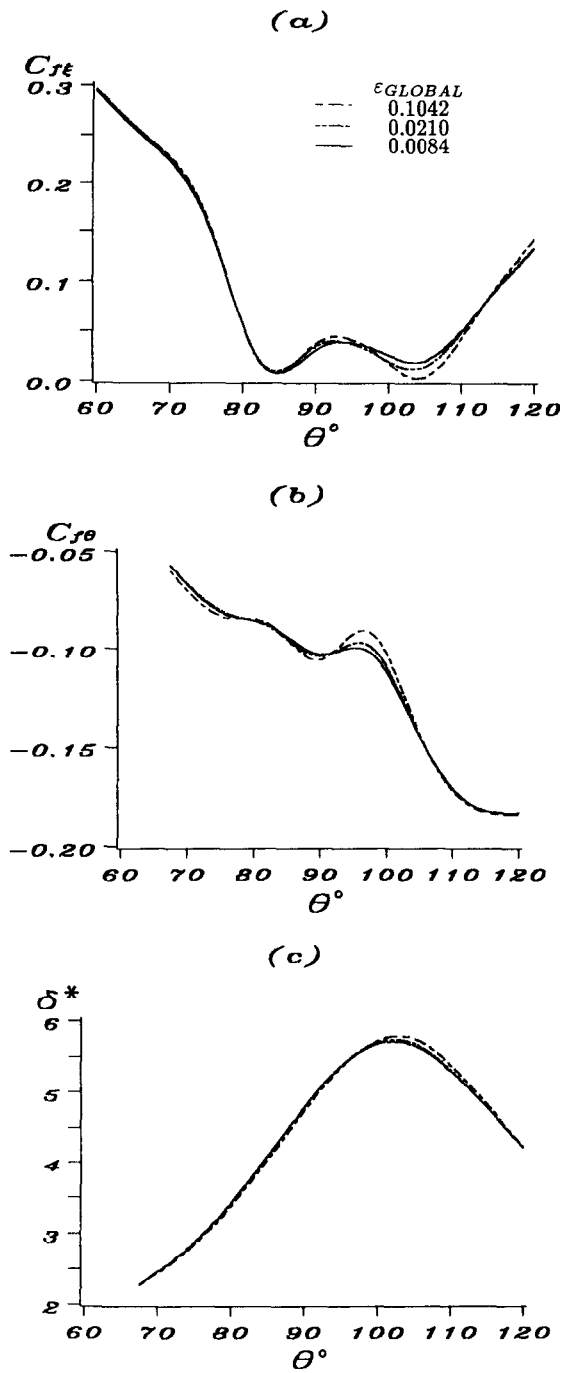

FIG. 5. The effect of the global iteration's convergence criterion on the solution.

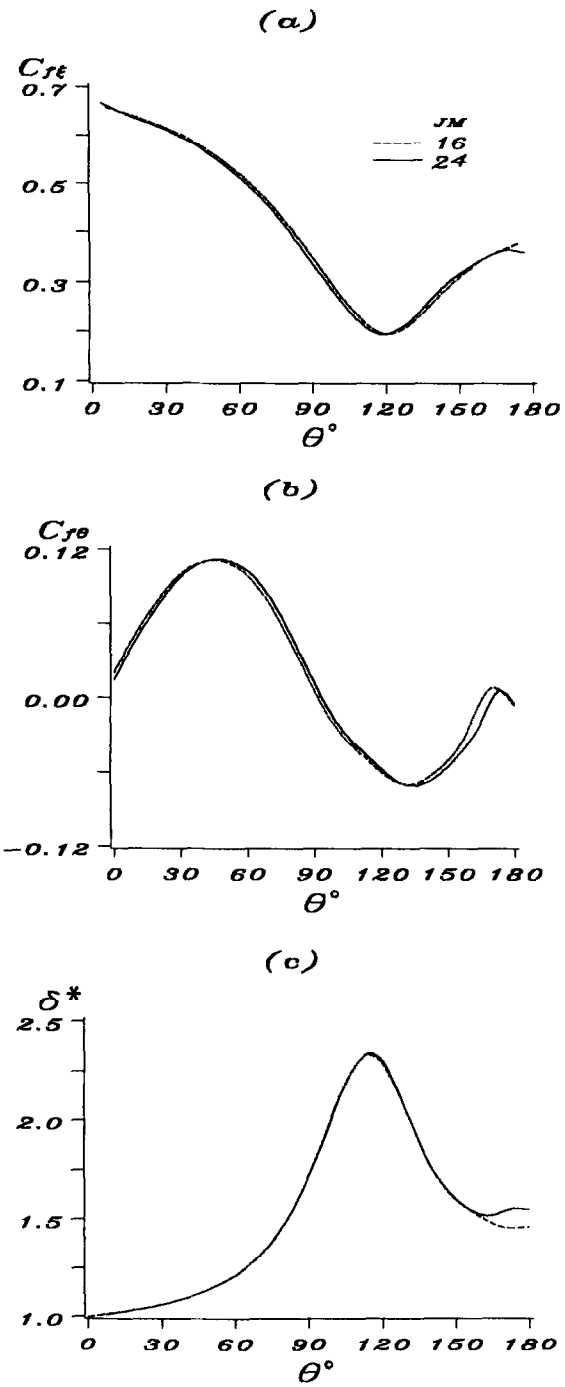

FIG. 6. The solution for $JM = 16$ and $JM = 24$.

vergence with the t-mesh-size was found for the quantities tested, as expected for a first-order accurate scheme. The differences in the solutions were insignificant for $NM > 24$.

A similar convergence test could not be pursued in the crossflow directions because of the excessive computing time required. Some partial tests have been made by employing two meshes with a different number of mesh points in the q-direction, $IM = 16$ and $IM = 24$, see Fig. 6, or in the s-direction, $JM = 16$ and $JM = 24$, see Fig. 7. The differences between the solutions are small, proving that in the present domain of solution a moderate number of grid points may yield reasonable solutions.

The amount of first-order numerical diffusion added to the central difference approximation of the lateral convection terms depends on the parameter ε in (10). At small angles of attack no artificial dissipation is required ($\varepsilon = 0$). At larger incidences, significant circumferential velocity is developed and numerical dissipation should be switched on ($\varepsilon > 0$). Diagonal dominance is assured if $\varepsilon = 1$ (upwind approximation), and smooth solutions are obtained for all Reynolds numbers at the cost of increased numerical diffusion. Several numerical experiments have been conducted in the present study to investigate the influence of the numerical diffusion. These experiments show that the degradation in the accuracy of the results is acceptable for the cases studied in this work. Figure 8 compares the solutions obtained for $\varepsilon = 0$ and $\varepsilon = 1$, for a 6:1 spheroid at the section $Z = 0.142$ at a moderate angle of attack (10°) and a Reynolds number of 1.6×10^6. At this crossflow section the circumferential component of the velocity is moderate and no significant differences can be detected between the two cases. Some disagreement can be found for $C_{f,\xi}$ and δ^* near the symmetry planes where the boundary layer is relatively thin and therefore the resolution of the first-order scheme might be insufficient.

At higher incidence, the crossflow velocity is large and the numerical dissipation may adversely affect the solution. In these cases, the first-order accuracy is unacceptable (see also Section 6). The present work considers only cases with intermediate incidences and therefore the choice $\varepsilon = 1$, along with an adequate number of mesh points and a close outer boundary, is acceptable. The mesh spacing in the normal direction is small since the outer boundary is relatively close to the spheroid. Hence, sufficient resolution of the boundary layer is obtained even with the first-order scheme.

5.3. *Effect of the Boundaries Location*

Some tests have been conducted to study the effect of the location of the boundaries. All the cases presented in this section refer to a 4:1 spheroid at an incidence of 6° and $\mathrm{Re} = 10^6$. Figure 9 shows the distribution of the skin-friction coefficients and the integral thickness δ^* at two axial sections, $\theta = 90°$ and $\theta = 135°$. At each case, three different locations of the upstream, (Z_i), downstream (Z_f) and outer boundary ρ_{out} are considered (the surface of the spheroid is at $\rho = 0.255$). In the

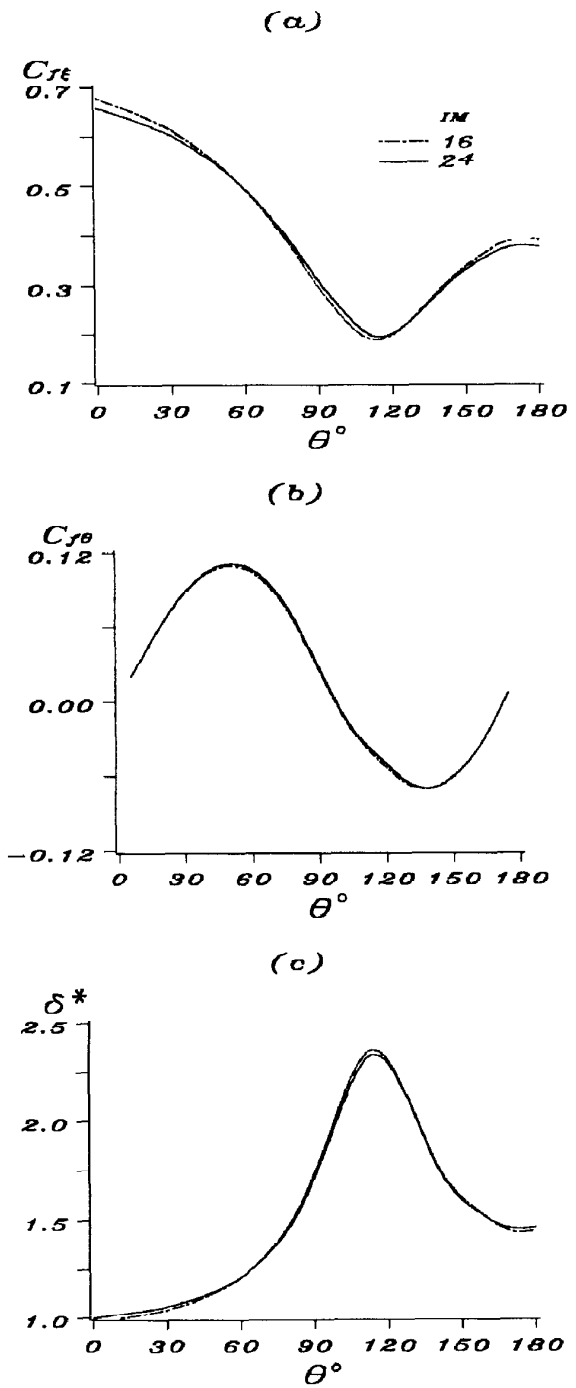

FIG. 7. The solution for $IM = 16$ and $IM = 24$.

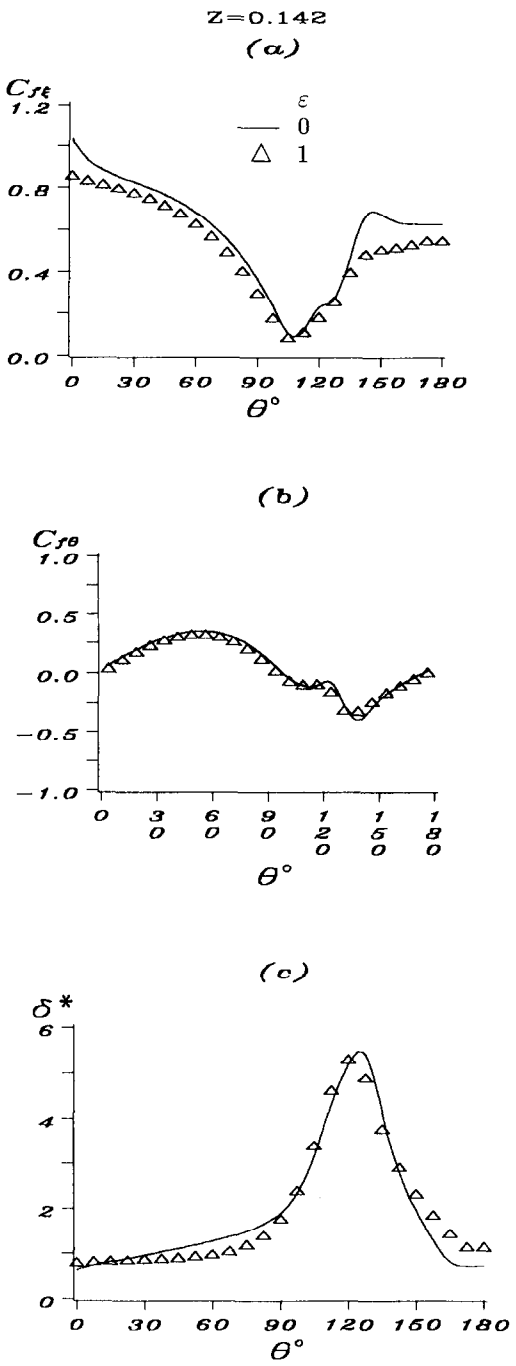

FIG. 8. The effect of the numerical diffusion on the solution.

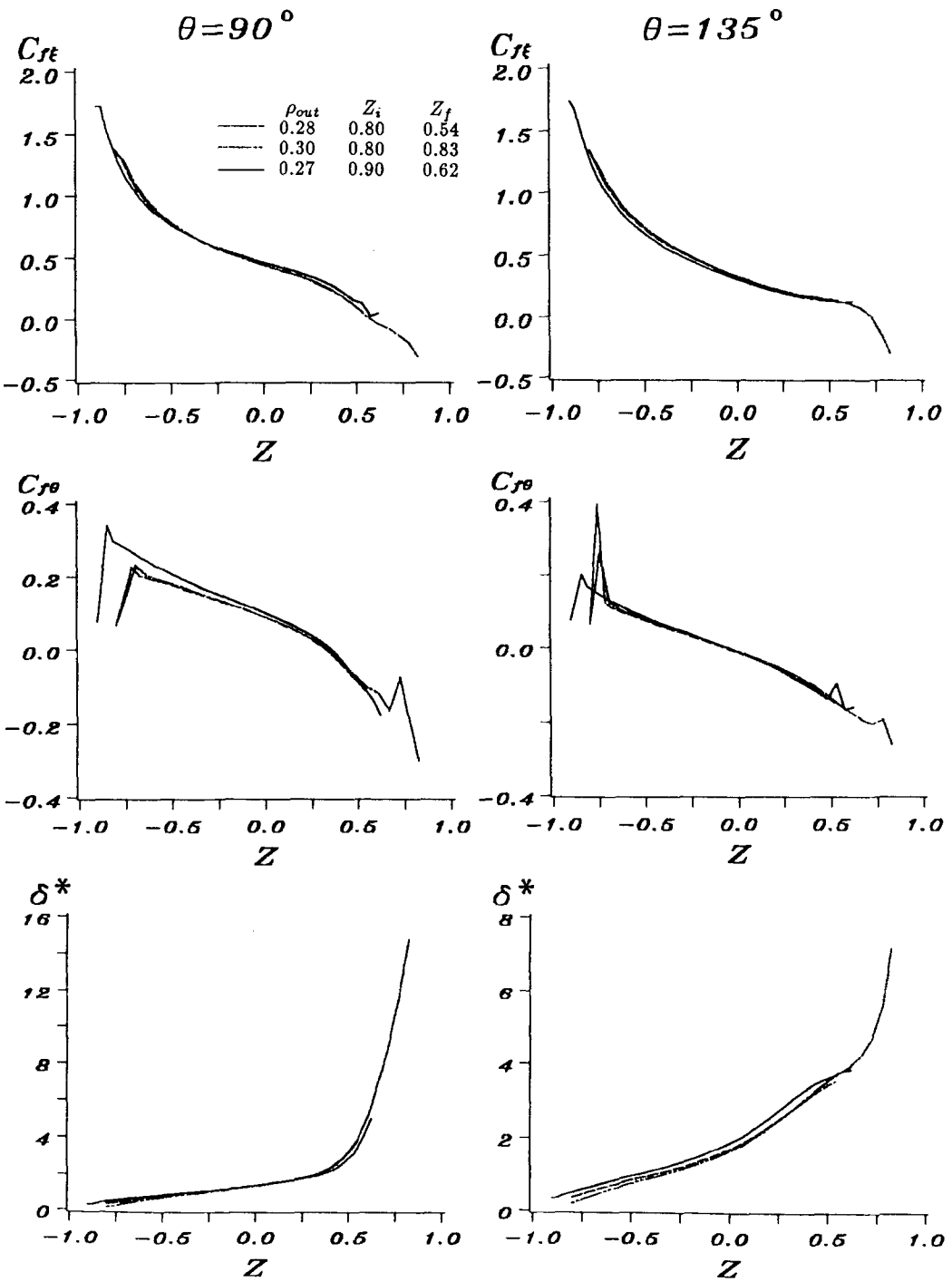

FIG. 9. The effect of the boundaries location on the solution.

major parts of the computational domain the solution is found to be independent of the location of the boundaries.

Some oscillations near the upstream boundary can be observed in Fig. 9. The origin of these oscillations cannot be precisely identified. However, certain facts may suggest that it is related to the boundary conditions chosen for the circumferential velocity at the upstream boundary. As the reader may recall, the streamwise velocity profile has been specified from an integral boundary layer solution, while the two crossflow components of the velocity have been approximated from the potential solution. The boundary layer approximation is a reasonably accurate condition and therefore the streamwise component of the skin friction is less sensitive to the location of the upstream boundary and no oscillations are generated. However, it appears that the potential approximation of the crossflow velocity components at the upstream boundary is less acceptable. Anyway, this behavior of the circumferential skin friction seems to have only a local effect which does not affect the solution downstream.

Some oscillations are observed also near the downstream boundary at $130^\circ > \theta > 90^\circ$. This region is characterized by a very rapid growth of the boundary layer thickness (see the distribution of δ^*) and the assumption that no interaction exists between the outer inviscid region and the viscous solution is not valid. Several numerical experiments have shown that if the outer boundary is placed inside the viscous region, oscillations occur and the iterative solution scheme may even diverge. These oscillations disappear when the outer boundary is moved into the inviscid (or even better, into the potential) region.

One point should be re-emphasized: the RNS as well as the TL approximations are not singular near flow separated zones. All the indications tested suggest that the irregular solution near the downstream boundary is a result of the placement of the outer boundary in a strong viscous–inviscid interaction region, combined with the prescription of the pressure as a boundary condition (see also Sections 1 and 6).

5.4. *Flow Field Solutions*

The present paper focuses on the description of the solution method of the three-dimensional RNS equations in generalized orthogonal curvilinear coordinate systems. Yet, some solutions of the flow field over slender spheroids at incidence will be briefly presented to demonstrate the capabilities of the procedure.

Figure 10 compares the shear-stress vector plot with the experimental results of Kreplin *et al.* [6] for a flow over a 6:1 prolate spheroid at an incidence of 10° and a Reynolds number of 1.6×10^6 (based on the length of the spheroid). A grid of $24 \times 24 \times 32$ mesh points was employed in the normal, circumferential, and axial directions, respectively, with grid points clustered near the surface of the spheroid. It was found experimentally by Kreplin *et al.* [6] that most of the flow field is laminar except in regions of flow separation. In the laminar regions of the flowfield the agreement is usually good, bearing in mind the complexity of the flow field and the difficulties associated with measuring the skin friction in laminar regions

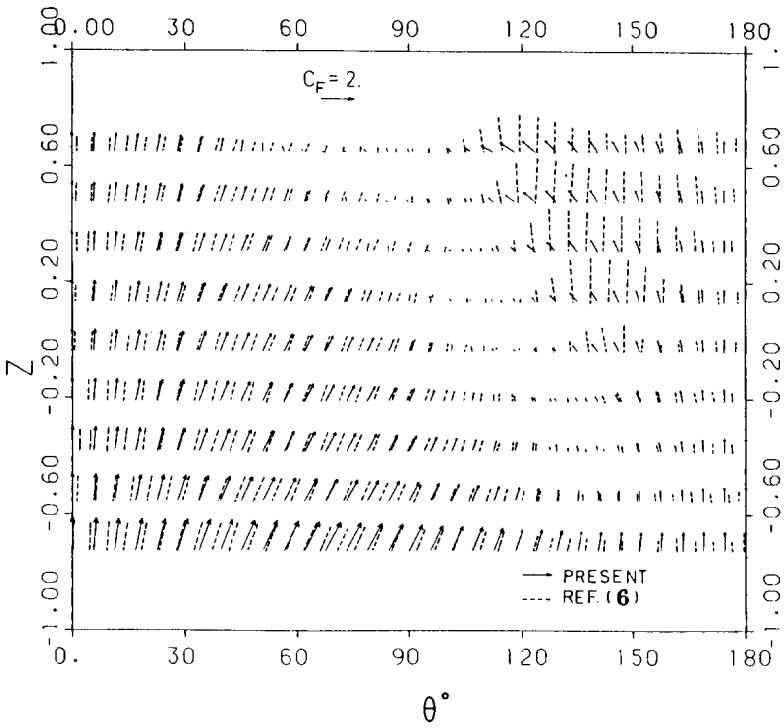

FIG. 10. Comparison of the skin-friction coefficient vector on the spheroid with experimental results.

(Kreplin *et al.* [6]). The agreement at the upstream boundary near the leeward side is not as good. This is attributed to inaccurate upstream boundary conditions used in the present calculations (see Section 5.3). Indeed, this effect is local and the agreement near the leeward symmetry boundary improves at the downstream parts. The results are, in particular, in disagreement at the downstream stations, leeward of the line of zero circumferential skin friction. The drastic increase of the shear stress in the experimental results is due to transition to a turbulent flow in this

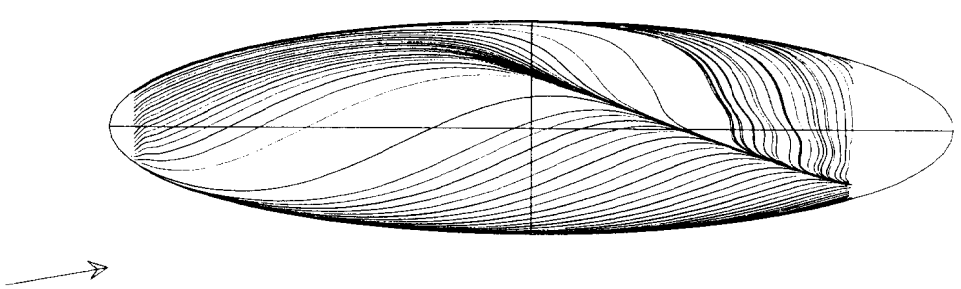

FIG. 11. Skin-friction lines on a 4:1 prolate spheroid at 10° incidence.

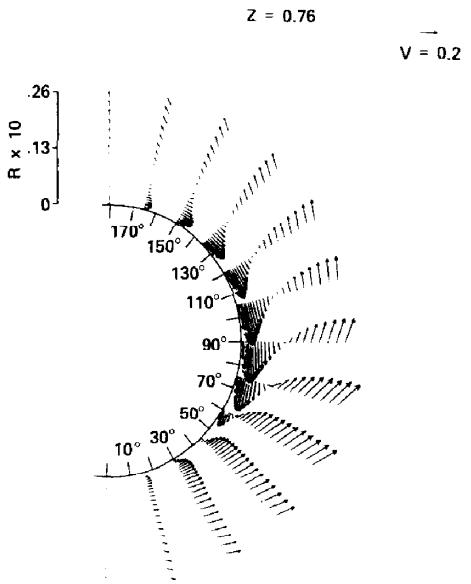

FIG. 12. The velocity field at the crossflow plane $Z = 0.76$ for a 4:1 prolate spheroid at 10° incidence.

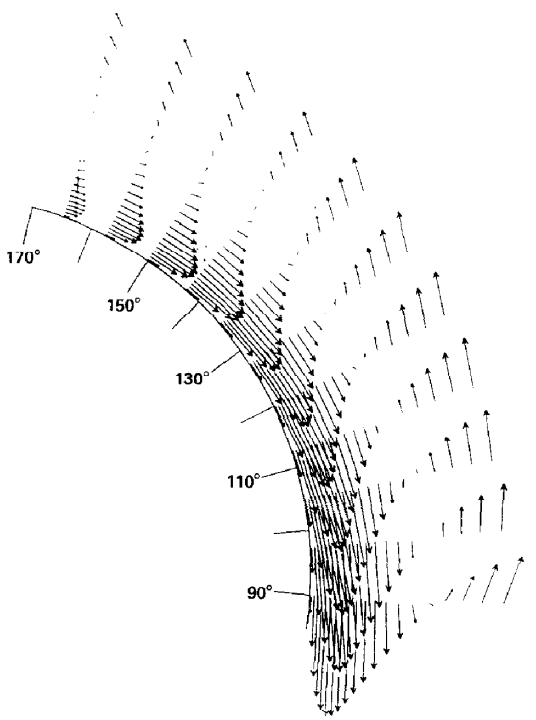

FIG. 13. Enlargement of the velocity field at the leeward side of the crossflow plane ($Z = 0.76$).

region. Obviously, the present laminar calculation cannot reproduce such a phenomenon.

Figure 11 gives the skin-friction lines (which coincide with the limiting streamlines) for the flow over a 4:1 spheroid at an incidence of 10° and $\mathrm{Re} = 10^6$. A mesh similar to the previous case has been used. At the second half of the body, the skin-friction lines appear to convergence into a swept line, which might be the separation line of a longitudinal vortex. Near the downstream boundary the flow is reversed along the mainstream direction. Figure 12 shows the projection of the velocity vector on the crossflow plane $Z = 0.76$. The scale of the normal distance from the spheroid surface, ρ, is enlarged five times and only every second circumferential line is plotted for clarity. Figure 13 shows an enlarged view of Fig. 12 on the leeward side of the spheroid (here every circumferential line is shown). Substantial regions with circumferentially reversed flow can be found, but the onset of a vortex flow cannot be clearly observed.

6. Concluding Remarks

An efficient solver of the three-dimensional, steady, and incompressible RNS equations in primitive formulation is presented for curvilinear orthogonal coordinate systems. The discrete equations are solved by a plane-by-plane iterative marching method. The algebraic equations in each crossflow plane are solved simultaneously by a preconditioned GMRES method without any splitting errors. The iterative solution method has numerical properties similar to the SPOR method for the solution of a single second-order elliptic equation, while other existing solution methods have the less favorable convergence properties of Jacobi-type iterative schemes. The good smoothing rates may be utilized to considerably reduce the computational time by employing multi-grid methods. Even without the implementation of a multi-grid solver, the required computational resources in terms of storage and CPU time allowed a solution of a relatively complicated flow field using a medium size scalar computer.

Although the method is designed for the RNS equations, it can be extended to the solution of the full Navier–Stokes equations. The streamwise diffusion can be incorporated implicitly during the marching process (the downstream value of the velocity can be taken from the previous global iteration) or explicitly as a source term (which can be computed from the previous global iteration). This solution strategy may work equally well for the unsteady case by solving each time step by the present iterative, space-marching method. The present method may be a good alternative to the well-known artificial compressibility or fractional-step methods.

A series of numerical experiments have been used to test the solution procedure and several of its properties. It is well established that second-order stable schemes result in more accurate solutions. Nevertheless, the present work obtains only first-order accurate solutions at high Reynolds numbers for the sake of stability. It has been shown that for moderate incidences and an adequate choice of the computa-

tional domain, the solutions obtained are acceptable. The accuracy of the method can be increased to second order by a Richardson extrapolation or double discretization (deferred correction) method without degrading the stability properties. The last method can be implemented relatively easily by using the first-order accurate scheme as the preconditioner of the GMRES method, but computing the residuals by a second-order-accurate approximation. This topic will be the subject of a future study.

Numerous solutions of the TL equations obtained by other researches demonstrate that this approximation is not singular at separation. The same should apply to the RNS equations, which are a more complete approximation of the Navier–Stokes equations. However, the solutions may suffer a numerical instability or singular behavior when the outer boundary is located in regions of strong viscous–inviscid interaction. The source of the instability may be related to the prescription of the pressure at the outer boundary. Two remedies can be suggested: (i) moving the outer boundary out of the strong interaction region or (ii) using an interactive scheme where the viscous region affects the inviscid solution.

In the two-dimensional case, Rosenfeld and Israeli [10] have shown theoretically and numerically, the superiority of the present method over conventional RNS solution methods which do not introduce a correction term of the type (14). The efficiency of the present three-dimensional solution method in comparison with other available methods has not been tested numerically. However, the present space-marching scheme is expected to be more efficient from the computational point of view, since it is constructed to be equivalent to a Gauss–Seidel iterative scheme while the other solution method are equivalent to a Jacobi-type iterative scheme. In the case of the RNS equations, the present method is also more economical in terms of storage because only one three-dimensional array (the pressure field) has to be stored.

The efficiency of the present method may be further improved if a line iterative scheme could be devised instead of the plane iterative scheme. However, it is not clear yet how a simple modification of the type (14) can be introduced so that the solution scheme of the continuity and momentum equations will be equivalent to a SLOR iterative scheme for the solution of a Poisson-like equation.

Appendix A

The present appendix gives some details on the solution of the linear system of equations (13) by a preconditioned GMRES algorithm [21]. Equation (13) is written as

$$(Q^{-1} M)\, \Delta\phi = (Q^{-1} b), \tag{A1}$$

where for simplicity the indices n and k are omitted. In the present work, the preconditioning matrix Q is chosen to be a block approximate factorization method.

The application of the GMRES method, without explicitly computing Q^{-1}, results in the following algorithm.

Given an approximation $\Delta\phi^l$ to (A1) ($\Delta\phi^0 = 0$), one cycle of GMRES advances the solution by first choosing k orthonormal search directions $p_1, p_2, ..., p_k$ as follows:

Compute residual

$$r^l = b - M\Delta\phi^l. \tag{A2}$$

Find

$$p_1 = r^l. \tag{A3}$$

Normalize

$$p_1 = p_1 / \| p_1 \|. \tag{A4}$$

Compute

$$d_1 = Mp_1. \tag{A5}$$

For $j = 1, 2, ..., k-1$, compute

$$Qe_j = d_j. \tag{A6}$$

Find an orthonormal search direction p_{j+1} from

$$p_{j+1} = e_j - \sum_{i=1}^{j} b_{ij} p_i, \tag{A7}$$

where

$$b_{ij} = q_j \cdot p_i, \tag{A8}$$

such that

$$(p_{j+1}, p_i) = 0 \qquad \text{for} \quad i = 1, 2, ..., j. \tag{A9}$$

Normalize

$$p_{j+1} = p_{j+1} / \| p_{j+1} \|. \tag{A10}$$

Compute

$$d_{j+1} = Mp_{j+1}. \tag{A11}$$

The vectors r_j, p_j, e_j, d_j are of length J, where J is the number of unknowns in a crossflow surface.

The updating of $\Delta\phi$ is done by

$$\Delta\phi^{l+1} = \Delta\phi^{l} + \sum_{i=1}^{k} a_i p_i, \tag{A12}$$

where the coefficients a_i minimize the residual norm (r_i, r_i). The minimization leads to the least squares problem

$$Da_i + B_i = 0, \tag{A13}$$

where the terms of the matrix D are given by

$$D_{ij} = d_i \cdot d_j \tag{A14}$$

and the vector B is computed from

$$B_i = d_i \cdot r^l. \tag{A15}$$

The GMRES method has good convergence properties, but requires substantial additional storage for the $2k$ vectors p_j, d_j. The storage requirements could be decreased (but the computational work would be increased) by storing only p_j and computing d_j from (A6), (A7). The convergence of the method improves with k, but the storage and computational requirements increase. In the present work, $k = 20$–30 is found to be optimal.

The present implementation uses a normal form of the equations to solve the least squares problem. Recently, more stable methods of solving the least squares problem have been suggested, see for example [15, 20]. The convergence properties of the present GMRES implementation have been found to be satisfactory (probably due to the preconditioning) and therefore the use of the new, more sophisticated, and computationally expensive procedures were not required.

ACKNOWLEDGMENTS

The research was partially supported by Stiftung Volkswagenwerk Grant I/37270. The second author was partially supported by DARPA N0014-86-K-0759 and ONR N0014-82-C-0451. The authors thank the reviewers for their helpful comments.

REFERENCES

1. R. J. BODONYI AND P. W. DUCK, *Comput. Fluids* **16**, 279 (1988).
2. A. J. CHORIN, *J. Comput. Phys.* **2**, 12 (1967).
3. A. J. CHORIN, *J. Math. Comput.* **22**, 745 (1968).
4. M. ISRAELI AND A. LIN, *Comput. & Fluids* **13**, 397 (1985).

5. J. KIM AND P. MOIN, *J. Comput. Phys.* **59**, 308 (1985).
6. H. P. KREPLIN, H. VOLLMERS, AND H. U. MEIER, *Z. Flugwissensch. Weltraumforsch.* **6**, 248 (1982).
7. Y. KRONZON, I. PARTOM, AND M. WOLFSHTEIN, *in* "Proceedings, 2nd International Conference on Numerical Methods in Laminar and Turbulent Flows, Venice, 1981," edited by C. Taylor and B. A. Schrefler (Pineridge, Swansea, 1981), p. 955.
8. D. KWAK, J. L. CHANG, S. P. SHANKS, AND S. CHAKRAVARTHY, *AIAA J.* **24**, 390 (1986).
9. M. ROSENFELD, Thesis, Technion-Israel Institute of Technology, 1986 (unpublished).
10. M. ROSENFELD AND M. ISRAELI, *AIAA J.* **25**, 641 (1987).
11. M. ROSENFELD, M. ISRAELI, AND M. WOLFSHTEIN, *AIAA J.* **26**, 129 (1988).
12. S. G. RUBIN, *in* "Proceedings, Ninth International Conference on Numerical Methods in Fluid Dynamics, Paris, 1986," edited by Soubbaramayer and J. P. Boujot (Springer-Verlag, Berlin, 1984), p. 62.
13. S. G. RUBIN AND A. LIN, *Israel J. Technol.* **18**, 21 (1980).
14. S. G. RUBIN AND D. R. REDDY, *Comput & Fluids* **11**, 266 (1983).
15. Y. SAAD AND M. SCHUTZ, *SIAM J. Sci. Stat. Comput.* **7**, 856 (1986).
16. W. SCHÖNAUER AND K. HÄFELE, *Comput. & Fluids* **15**, 93 (1987).
17. H. W. STOCK, *Z. Flugwissensch. Weltraumforsch.* **4**, 217 (1980).
18. W. R. VAN DALSEM AND J. L. STEGER, "The Efficient Simulation of Separated Three-Dimensional Flow Using the Boundary Layer Equations," AIAA Paper 85-4064, 1985 (unpublished).
19. A. E. P. VELDMAN, *AIAA J.* **19**, 79 (1981).
20. H. F. WALKER, *SIAM J. Sci. Stat. Comput.* **9**, 152 (1988).
21. L. B. WIGTON, N. J. YU, AND D. P. YOUNG, "GMRES Acceleration of Computational Fluid Dynamics Codes," AIAA Paper 85-1494, 1985 (unpublished).